IEEE Journal of Translational Engineering in Health and Medicine

Received 26 October 2023; revised 9 February 2024; accepted 19 February 2024.
Date of publication 20 February 2024; date of current version 1 March 2024.

Digital Object Identifier 10.1109/JTEHM.2024.3368291

A Wavelet-Based Approach for Motion Artifact Reduction in Ambulatory Seismocardiography

JAMES SKORIC, (Graduate Student Member, IEEE), YANNICK D'MELLO, AND DAVID V. PLANT, (Fellow, IEEE)

Department of Electrical and Computer Engineering, McGill University, Montreal, QC H3A 0E9, Canada

CORRESPONDING AUTHOR: J. SKORIC (james.skoric@mail.mcgill.ca)

This work was supported in part by the National Sciences and Engineering Research Council (NSERC), and in part by McGill University.

This work involved human subjects or animals in its research. Approval of all ethical and experimental procedures and protocols was granted by the McGill Research Ethics Board under Application No. 6-0619.

ABSTRACT Wearable sensing has become a vital approach to cardiac health monitoring, and seismocardiography (SCG) is emerging as a promising technology in this field. However, the applicability of SCG is hindered by motion artifacts, including those encountered in practice of which the strongest source is walking. This holds back the translation of SCG to clinical settings. We therefore investigated techniques to enhance the quality of SCG signals in the presence of motion artifacts. To simulate ambulant recordings, we corrupted a clean SCG dataset with real-walking-vibrational noise. We decomposed the signal using several empirical-mode-decomposition methods and the maximum overlap discrete wavelet transform (MODWT). By combining MODWT, time-frequency masking, and nonnegative matrix factorization, we developed a novel algorithm which leveraged the vertical axis accelerometer to reduce walking vibrations in dorsoventral SCG. The accuracy and applicability of our method was verified using heart rate estimation. We used an interactive selection approach to improve estimation accuracy. The best decomposition method for reduction of motion artifact noise was the MODWT. Our algorithm improved heart rate estimation from 0.1 to 0.8 r-squared at −15 dB signal-to-noise ratio (SNR). Our method reduces motion artifacts in SCG signals up to a SNR of −19 dB without requiring any external assistance from electrocardiography (ECG). Such a standalone solution is directly applicable to the usage of SCG in daily life, as a content-rich replacement for other wearables in clinical settings, and other continuous monitoring scenarios. In applications with higher noise levels, ECG may be incorporated to further enhance SCG and extend its usable range. This work addresses the challenges posed by motion artifacts, enabling SCG to offer reliable cardiovascular insights in more difficult scenarios, and thereby facilitating wearable monitoring in daily life and the clinic.

INDEX TERMS Heart rate monitoring, motion artifact reduction, seismocardiography, wavelets, wearable monitoring.

I. INTRODUCTION

CARDIOVASCULAR disease (CVD) is a major global health burden, contributing to significant morbidity and mortality rates worldwide [1]. The continuous monitoring of cardiovascular health has emerged as a vital approach in addressing these challenges. Continuous monitoring allows for the detection of subtle changes and abnormalities that might go unnoticed during an intermittent medical evaluation [2]. This approach enables early detection of CVDs, allowing for timely interventions and personalized treatment plans [3]. By leveraging continuous monitoring technologies, healthcare professionals can enhance the prevention, diagnosis, and management of CVD, ultimately improving patient outcomes and quality of life [4]. However, traditional methods often require complex equipment which limits mobility and are unsuitable for monitoring outside of the clinic [5]. In recent years, wearable monitoring devices have emerged as a promising solution that enables the non-invasive monitoring of various physiological parameters in real-time.

Wearable monitoring devices have revolutionized healthcare by providing continuous and personalized monitoring systems [6]. These devices have gained significant popularity

due to their convenience, mobility, and real-time data collection capabilities. Wearable devices come in various forms, such as smartwatches, fitness trackers, and patch-like sensors, which can be worn comfortably for extended periods. These devices can provide a comprehensive picture of cardiovascular health by continuously tracking variety of biometric parameters [7].

Seismocardiography (SCG) is an innovative wearable technique that has gained significant attention in the field of cardiovascular monitoring [8]. SCG captures the vibrations produced by the mechanical activity of the heart. These vibrations enable a real-time, central, and non-invasive assessment of cardiac performance [9] enabling valuable insights into cardiac function. By measuring the vibrations associated with each heartbeat, SCG can monitor heart rate [10], [11], detect abnormalities [12], classify atrial fibrillation [13], and predict heart failure [14]. Furthermore, key fiducial points in the SCG waveform have been associated with valve movements [15], [16], enabling the measurement of cardiac time intervals such as left-ventricular ejection time [17], [18], and pre-ejection period [19], [20]. SCG has also been used to derive information on stroke volume [21], and respiratory information [22]. Since the SCG sensor requires only a single point of contact, it eliminates the need for multiple electrodes or sensors attached to different parts of the body, thereby simplifying the monitoring process and enhancing user comfort. These human-focused design features enable SCG to surpass the low acceptance rate of other wearables [23], which is a consistent barrier in patient monitoring [24]. By providing comprehensive cardiac insights and integrating various physiological measurements, SCG improves the convenience, accuracy, and accessibility of cardiovascular monitoring. These capabilities have direct clinical applications in the diagnosis, management, and prevention of cardiovascular diseases, enabling personalized interventions, and remote patient monitoring for enhanced cardiovascular care.

The decades of use of electrocardiography (ECG) based Holter monitors underscore the importance of long-term, wearable monitoring of physiological parameters during daily life. SCG, by design, is targeted for wearable monitoring applications and can offer a distinct perspective of cardiac mechanics that extends beyond what ECG alone can capture. However, the dynamic nature of daily life introduces a myriad of environmental and physiological factors that can complicate the accurate and meaningful interpretation of wearable SCG data. Unfortunately, a significant portion of SCG research has been conducted in controlled laboratory settings where artifacts are minimized. As a result, the accuracy of SCG cannot yet compete with Holter monitors in clinical settings. In this context, design of a system that can withstand dynamic environments is crucial towards the clinical translation of SCG. This would enable the content-rich analysis of cardio-mechanical activity to the extent that current alternatives cannot provide. Recording SCG in daily life poses challenges due to the presence of motion artifacts. Activities like walking, running, and even normal body motions introduce noise and artifacts into the SCG signal, obstructing the accurate capture and analysis of cardiac data. These artifacts not only compromise the quality of the SCG signal but also impede the extraction of valuable information regarding cardiac function due to the strength of the vibrations. Thankfully, with appropriate processing techniques, it should become possible to recover the original cardiac signal provided there is no clipping from the accelerometer. However, due to the stochastic nature of motion artifacts and the variability of SCG, the task is more complex than it may initially seem and necessitates advanced processing techniques.

There have been several attempts to reduce the effect of motion artifact on SCG signals. They generally incorporate either adaptive filtering [25], signal decomposition [26], or blind source separation [27]. The state-of-the-art algorithms can be grouped into two categories: ECG-assisted algorithms and ECG-less algorithms. Algorithms that are assisted with ECG are the most powerful in reducing motion artifacts. This is because ECG is more motion resistant than SCG [28]. They are useful to extract precise waveforms or timing of fiducial points. Unfortunately, they usually require some form of ensemble averaging, which negates any beat-to-beat analysis and heart rate (HR) monitoring. Di Rienzo et al. [29] proposed a method for wearable SCG that used ensemble averaging to extract cardiac time intervals such as pre-ejection period (PEP) and left-ventricular ejection time from the SCG waveform. Javiad et al. [30] used an empirical mode decomposition (EMD) on ensemble averaged beats for PEP detection. Lin et al. [31] used ensembled EMD (EEMD), paired with a sliding autocorrelation and compares it with ECG-derived HR and a quality factor, to limit artifactual beats. The EEMD is computationally expensive, plus artifactual periods are discarded and could result in a loss of data. Additionally, the method was only evaluated on vibrations from a moving subway car. Yang and Tavassolian [27] used constrained independent component analysis on several SCG sensors using the R-peak timing as a reference source waveform. This approach increases hardware complexity by requiring at least three electrodes when compared to the single sensor SCG technique.

For standalone SCG applications, ECG-less algorithms are preferred to minimize hardware complexity and maximize the autonomy of SCG. These algorithms are less functional, and generally give less detailed results towards specific cardiac timings. Pandia et al. [32] used a Savitsky-Golay filter to subtract motion artifact from SCG. Yang and Tavassolian [25] used a nonlinear least-means-squared filter where a delayed input of the SCG signal was used as the target reference. Yu and Liu [33] used a recursive-least-squares filter where a bandpass filtered SCG signal was used as the desired reference. The difficulty with adaptive filtering is that the methods hinge on producing a reliable estimate of the desired signal. Choudhary et al. [34] used wavelet decomposition with kurtosis and dominant frequency criteria used to select sub-bands

for aortic opening detection. While the original paper did not specifically propose the algorithm for motion artifacts, it was analyzed with respect to motion [31] however kurtosis could be a poor option in this application as vibrations from footsteps also exhibit high kurtosis [35].

SCG is a promising solution for cardiac monitoring thanks to its simplicity, compact form factor, and ability to provide a wealth of information. However, it is still limited in real-world applications where noise artifacts are present, which inhibits its clinical use. Ambulatory recordings remain a particular concern due to strong footstep related vibrations. To address this issue, this paper introduces a novel framework aimed at mitigating the effects of motion artifacts in SCG recordings. The proposed framework analyzes wave decomposition methods to effectively isolate the cardiac signal. Additionally, we demonstrate a noise suppression technique to further filter out residual unwanted noise. Finally, the effectiveness of the framework is assessed for HR monitoring during artificially corrupted walking data using a state-of-the-art HR algorithm. Through these analyses and evaluations, this study aims to advance the understanding and development of motion artifact reduction techniques in SCG-based remote cardiac monitoring.

II. METHODS

A. DATA ACQUISITION

Data collection took place at McGill University and was approved by the McGill Research Ethics Board (file number: 6-0619), approved August 12th, 2019. Prior written consent was obtained from all participants before their involvement in the study. The analysis involved two datasets. The first dataset consisted of five subjects who performed various walking and motion artifact inducing activities. A subset of this data was presented in [36] where HR estimation was performed on several different orientations while at rest. To capture cardiac vibrations and motion artifacts, two inertial measurement units (Invensense, MPU9250) were utilized. The first sensor was affixed to the xiphoid process of the sternum with a single piece of double-sided tape, as shown by the green box in Fig. 1. The X, Y, and Z axes were oriented in longitudinal, horizontal, and dorsoventral axes of the body. The second sensor was placed along the spine on the back of the body, in line with the main sensor on the front. Both inertial measurement units (IMU) were polled by a single Raspberry Pi Zero W using I2C protocol at approximately 270 Hz. Reference ECG signals were concurrently recorded using the BIOPAC system, and synchronization between ECG and IMU data was achieved using an externally hardwired clock from the BIOPAC to the Raspberry Pi.

Two one-minute recordings were obtained to introduce walking noise. During walking, subjects were instructed to walk in circles with a diameter of approximately 5 meters, at a comfortable speed of their choice. In one recording, the subjects walked clockwise and in the other they walked counterclockwise.

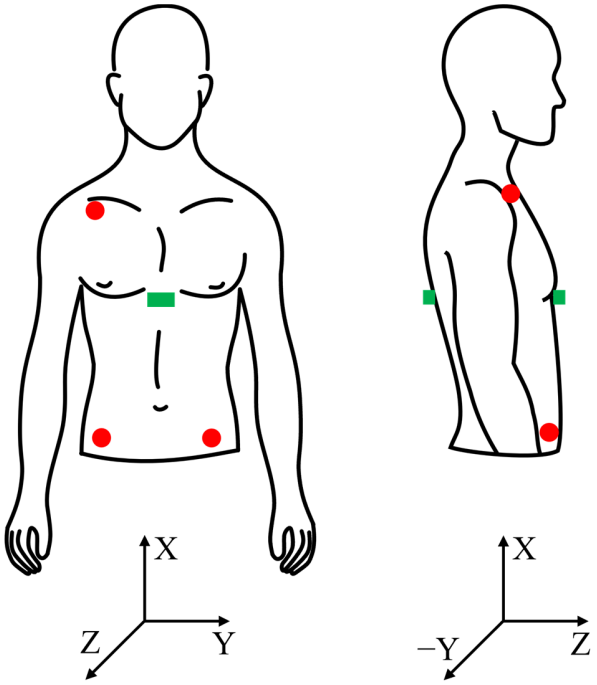

FIGURE 1. Position on the body for the IMU (green) and ECG (red) sensors with corresponding axes directions showing a front view (left) and side view (right).

The second dataset comprised sixty-two subjects with a single sternal IMU sensor. Subjects were recorded at rest in a supine position with no observed motion artifacts using the same sensor configuration as the first dataset. A subset of this data was discussed in [22]. Ten subjects were selected for analysis in this work based on the strongest cardiac amplitudes to confirm that any estimation inaccuracies were caused due to motion artifact noise, and not due to poor signal quality. Previous studies have demonstrated that the cardiac signal is primarily found in the acceleration-Z (AZ) and gyration-x (GX) axes [11]. Cardiac amplitudes were determined by calculating the root-mean-squared (RMS) amplitude of the ensemble average for the AZ and GX axis. The RMS values were sorted to rank the strongest AZ and GX signals, and the average of the two ranks was used to identify the ten subjects with the highest cardiac amplitudes.

Evaluating the performance of the algorithm can be challenging without a clear reference source. To establish an evaluation testbed, an artificially corrupted dataset was created. This was generated by adding the back sensor from the walking recordings to the clean data from the supine subjects. This approach relies on the assumption that the torso is rigid, resulting in similar external vibrations when recorded on the front or back of the torso. Additionally, it was assumed that the back location lacks sufficient cardiac signal for detection by the IMU, as demonstrated in [37]. Both claims were confirmed in our own datasets. Consequently, the back sensor served as a reliable estimate of the motion artifact noise source. Each of the ten resting recordings was

then corrupted by the ten walking datasets, resulting in a total of 100 unique permutations corresponding to 6000 seconds for analysis. This enabled a broad dataset of varying SCG profiles, signal strength, noise levels, and overlap across each permutation.

B. ALGORITHM OVERVIEW

The algorithm consisted of three main blocks. First, a decomposition block was used to isolate relevant cardiac-related elements. Then a time-frequency (TF) analysis was used to suppress remaining unwanted features by masking and nonnegative matrix factorization. Finally, our previously published autocorrelated differential algorithm (ADA) [10] for was used to evaluate the performance of the motion artifact reduction by heart rate estimation. The algorithm and analysis were developed in MATLAB 2022b using the signal processing, wavelet, and statistics toolboxes.

C. SIGNAL DECOMPOSITION

The first stage of the algorithm is to perform signal decomposition on the acceleration data. Signal decomposition is a process that involves breaking down a complex signal into its constituent components or building blocks. The goal of signal decomposition is to extract the underlying information contained within the signal and separate it for further analysis or processing. In an ideal setting, it would separate the cardiac-related information from the motion artifact related information. However due to the similarity of the vibrations from both sources – occurring with overlap in frequency and time characteristics, it is not trivial to isolate each one in this scenario. Therefore, we analyzed two decomposition methods from current state of the art and two new methods to determine which can best reconstruct the cardiac signal from the corrupted data.

The first method analyzed was empirical mode decomposition (EMD). EMD is a data-driven signal processing technique that enables adaptive decomposition of a complex signal into its intrinsic modes functions (IMF) by identifying local oscillatory components [38], and has previously been used for SCG [30]. These IMFs are obtained through a sifting process that extracts oscillatory behaviors from the original signal. Effectively, the EMD decomposes the acceleration signal into a set of IMFs that collectively represent the entire signal while individually representing different components relating to either cardiac or motion information. EMD extracts the IMFs from high to low frequency. We observed that the cardiac related content was primarily found in the first two IMFs, corresponding to the two highest frequency IMFs. The SCG waveform was reconstructed by summing these two IMFs.

The second decomposition method analyzed was the ensemble empirical mode decomposition (EEMD), which extends the capabilities of the EMD. EEMD addresses some limitations of EMD, such as mode mixing and sensitivity to noise [39], and has also been used previously for SCG [31]. EEMD involves generating multiple realizations, or ensemble members, of the input signal by adding white noise to the original data. Each ensemble member is then decomposed using EMD independently. After decomposing each ensemble member, the IMFs across all realizations are averaged to obtain the final set of IMFs. The advantage of EEMD lies in its ability to mitigate the impact of noise and enhance the separation of intrinsic modes, which can be particularly beneficial when dealing with non-stationary and noisy acceleration signals [39]. We analyzed EEMD in the same context as EMD, with the first two IMFs used for reconstructing the SCG signal.

The third evaluated method was the complete ensemble empirical mode decomposition with adaptive noise (CEEMDAN) algorithm. CEEMDAN is another EMD variation that extends the capabilities of EEMD by incorporating adaptive noise at each stage [40]. In EEMD, noise is added to the original data and then is fully decomposed, whereas in CEEMDAN, noise is added in each stage of the decomposition and a single residual is produced by averaging the IMF before proceeding to the next IMF. This results in a theoretically lower computational cost and a lower reconstruction error [40] – two important qualities when considering the proposed portability of SCG. As the same with the other two EMD-based methods, we used the two highest frequency IMFs to reconstruct the signal.

The final method analyzed in this work was a wavelet-based method. The discrete wavelet transform (DWT) decomposes a signal into different frequency components by applying a series of high-pass and low-pass wavelet filters [41]. The DWT operates in a multi-resolution framework, where the signal is successively down sampled and filtered at each level, resulting in a decomposition into multiple levels or scales. This hierarchical representation allows for a comprehensive analysis of the signal's frequency content across different resolutions.

In this work, we specifically examined the maximum overlap discrete wavelet transform (MODWT), a technique that extends the capabilities of the DWT. Unlike the DWT, MODWT does not down sample the signal at each scale. This causes the transform to be more redundant, less sensitive to the starting point, and applicable to any sample size at the cost of higher computational complexity [41]. The MODWT uses zero phase filters, which better preserve feature localization – critical for extracting cardiac timing indicators from the SCG waveform. Additionally, the transform is less sensitive to the selection of the wavelet filter [41]. The MODWT finds applications in various fields and is particularly useful for SCG analysis where a detailed and localized analysis of the signal's frequency content is required. In comparison to the EMD-based methods, MODWT was observed to better localize higher frequency bands, and therefore we observed the cardiac signal primarily in the first three sub-bands and these sub-bands were selected to reconstruct the cardiac signal. The sub-band selection was constant and were determined visually then confirmed numerically as the optimal number of sub-bands for signal reconstruction. This can be seen in Fig. 2

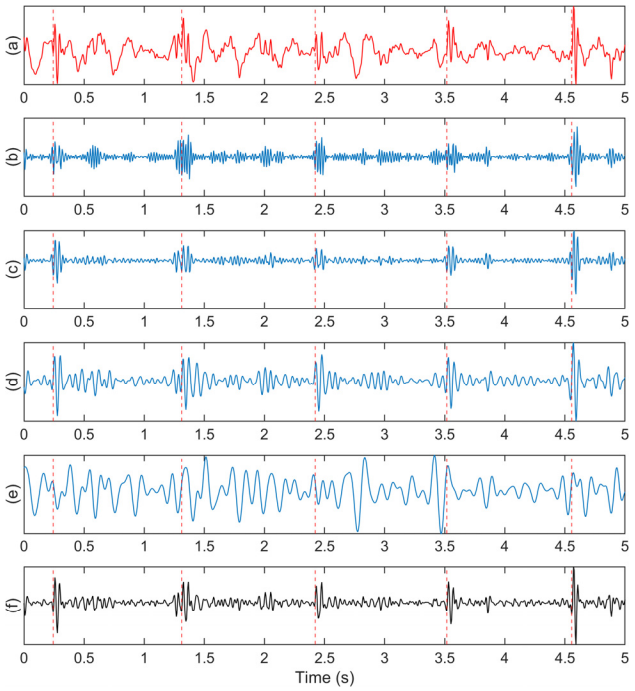

FIGURE 2. MODWT decomposition showing (a) input signal, (b) first sub-band, (c) second sub-band, (d) third sub-band, (e) fourth sub-band, and (f) reconstructed signal from first three sub-bands. ECG R-Peaks shown in red dashed lines.

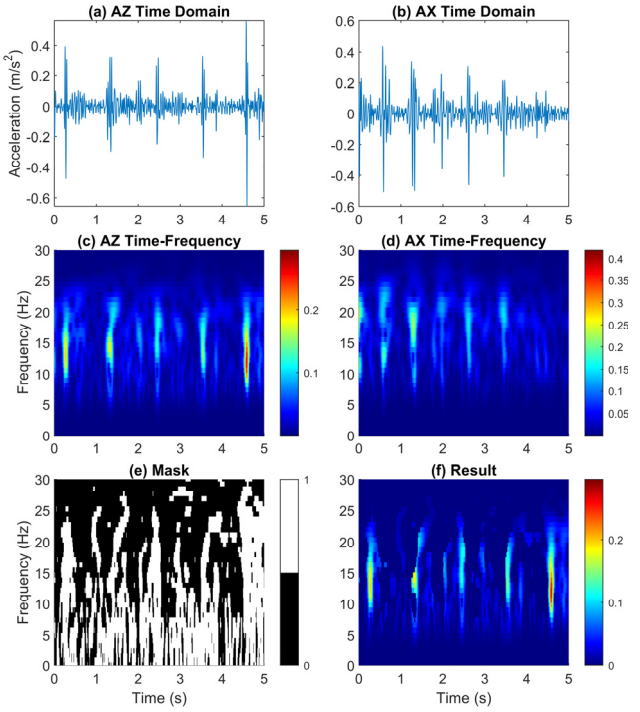

FIGURE 3. Demonstration of time-frequency masking showing (a) time domain of AZ axis, (b) time domain of AX axis, (c) CWT magnitude of AZ axis, (d) CWT magnitude of AX axis, (e) generated binary mask from the AZ and AX spectrums where a one is represented in white, and (f) AZ axis spectrum magnitude after the mask was applied.

where a five second period of the corrupted data is decomposed into several sub-bands via MODWT. For simplicity, only the first four out of fourteen sub-bands were shown, as they contained the most relevant information. The raw signal in Fig. 2 a) was decomposed, with the cardiac elements visible in plots Fig. 2 b) to Fig. 2 d) used to reconstruct the signal in Fig. 2 f). While this method separates out most of the cardiac and motion artifact, some remains, as evident by the erroneous vibrational pulse visible around at two seconds, which is unrelated to the heartbeat however is contained in the same frequency sub-band and therefore was not separated from the wavelet decomposition. This example highlights the need for further processing to suppress remaining additional vibrations that would be disruptive to sensitive processing algorithms.

D. ARTIFACT REMOVAL

1) TIME-FREQUENCY MASKING

Signal decomposition can separate signals well when there is a significant separation between the frequency bands and as a result, the out-of-band noise was removed from the signal. However there remains some in-band noise because of the overlap in the frequency distributions of the cardiac and motion related signals. Therefore, we implemented two methods to suppress the remaining in-band vibrations. For the first stage, we leveraged a technique commonly used in audio and speech processing known as time-frequency masking.

Time-frequency masking involves selectively attenuating or enhancing specific components of a signal in the TF domain [42], where the goal is to separate different sources in a mixture. TF masking utilizes the information in the TF representation of the signal, such as the continuous wavelet transform (CWT), or short-time Fourier transform (STFT), to identify and manipulate specific frequency components at different time intervals.

A binary mask can be created by comparing two TF representations. TF elements of the desired signal with an energy above that of the other source are assigned a 1 whereas those with a lower energy are assigned a zero. The binary mask can then be multiplied element-by-element to the target mixed signal to effectively suppress the regions corresponding to the unwanted source. In the context of ambulant SCG, the two sources can be represented as the cardiac signal, and the motion artifact. For a real-world application, we do not know the TF representations of either source so we must make an approximation. To approximate the noise, we used the accelerometer x-axis data as a noise estimate. Since the observed cardiac signal was much lower in the AX than the AZ axis, and the observed motion artifact was much higher in the AX than the AZ axis, the AX axis provided a fairly pure estimate of the motion artifact. First, the TF spectrums were generated for both the AX and AZ axes. A five-second-long example of each spectrum can be seen in Fig. 3 c) and d) for the AZ and AX, respectively. The two spectrums were compared to generate the binary TF mask shown in Fig. 3 e), with a 1 assigned when the energies of the AZ elements were

greater and a zero when the energies of the AX elements were greater. The two-dimensional mask was then applied to the AZ spectrum via element-by-element multiplication.

2) NONNEGATIVE MATRIX FACTORIZATION

The second technique to reduce unwanted vibrations was the Nonnegative Matrix Factorization (NMF). NMF is a commonly used and effective technique for breaking down complex matrixes into their essential components. Its unique prowess comes from the nonnegativity constraint, which makes it an optimal choice for applications such as separating sources in mixed audio signals [43]. The premise of NMF as an unsupervised learning technique is to decompose a nonnegative matrix into two lower-rank nonnegative matrices [44]. The product of these two lower-rank matrices should approximate the original matrix as seen in Equation 1 where C is the initial matrix, and W and H are the two factors.

$$C \approx W \times H \tag{1}$$

If C is a matrix with n-by-m dimensions, then the factor W will be of size n-by-k, and the factor H will be of size k-by-m with k representing the desired rank. The NMF technique iteratively updates the two matrices to minimize the difference between the original matrix and the approximation [45], [46]. By employing this powerful methodology for SCG, we can isolate motion artifacts from the invaluable cardiac data, resulting in clearer, more reliable signals. We implemented NMF to separate the TF spectrum magnitude into two sources as its spectrum satisfied the non-negativity criteria of NMF.

Unlike the TF masking technique, NMF is unsupervised and therefore does not require a noise estimate to function. However, due to the similarity of the two sources, if applied directly it would fail to recognize a distinction between them and would provide little improvement for either source. Our solution was to use the AX axis as an initial seed for the algorithm to assist the convergence towards something of a similar distribution. NMF was performed by the nnmf function in MATLAB which used an alternating least squares algorithm [46]. First, NMF was performed on the AX CWT spectrum, C_{AX}, to factorize the graph to two one-dimensional factors representing the time axis, H_x, and frequency axis, W_x, of the spectrum.

Next, NMF was performed on the AZ CWT spectrum, C_{AZ}, after the TF mask had been applied. H_x was used as an initial seed for the time-domain factor, H_0, of the NMF of C_{AZ}. The other initial factors were randomly initialized. The NMF on C_{AZ} factorized the signal into two factors, W_Z and H_z, each with a rank of 2. We can assume that each the two vectors in each factor represent a cardiac component and a noise component because the noise component was seeded with H_x.

Finally, a TF representation of the SCG-related signal, $\widehat{C}_{SCG}$, was generated by multiplying the first component from each factor. The inverse CWT was applied by using the magnitude defined by $\widehat{C}_{SCG}$ with the phase from the initial spectrum, C_{AZ} to reconstruct a time domain SCG-like representation, with suppressed motion artifacts.

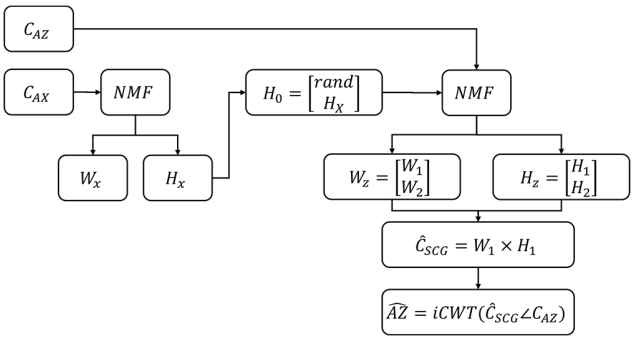

FIGURE 4. Flowchart of the developed NMF-based artifact reduction method. NMF of the AZ CWT spectrum, C_{AZ}, was initialized using a NMF decomposition of the AX CWT spectrum, C_{AX}. A SCG-like waveform, $\widehat{AZ}$, was reconstructed using the first component from each factor, and the original phase information.

3) PROPOSED ALGORITHM

Using the described techniques, we developed an optimized algorithm to reduce the motion artifacts corresponding to footsteps. An overview of the algorithm can be seen in Fig. 5. First, the acceleration data was resampled to 200 Hz and was bandpass filtered by a 3rd order Butterworth filter with 3dB cutoffs of 3 Hz and 50 Hz, which was sufficient in capturing the frequency range of SCG in line with previous studies [47]. Next, MODWT was used to decompose the signal, of which the three highest frequency sub-bands were selected to reconstruct the signal. The same decomposition was applied to both the AZ and AX axes.

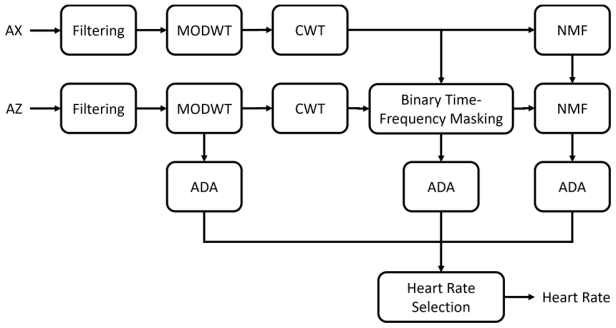

FIGURE 5. Flowchart of the developed algorithm. The same processing is done on both the AZ and AX axes, then the AX is used to improve the AZ by time-frequency masking and AX used as an initialization for the AZ NMF. ADA is computed at different stages of the algorithm then all estimates are concatenated, and a single heart rate estimation is produced.

Next, the time-frequency analysis was performed on the reconstructed signal. While the STFT, CWT, and wavelet synchrosqueezed transform (WSST) were evaluated, the CWT was implemented because it provided a better resolution of cardiac beats than the STFT and a much faster processing time than the WSST. The CWT was implemented on the AZ and AX axes to create a TF representation of the waveform for each axis. The binary TF masking was then performed on the AZ spectrum. Finally, the NMF stage was performed on the AZ spectrum, as initialized by the AX axis described

in section II-E, resulting in a waveform that has had motion artifact related vibrations significantly suppressed.

Each of these methods can fail at different timesteps of the signal, either in scenarios where the motion artifact was not adequately suppressed, or where the cardiac signal was suppressed too heavily. Therefore, HR estimation was performed on the signals probed at different stages in the reduction process – specifically after MODWT, TF masking, and NMF. HR was calculated using the ADA [10], which uses a windowing and autocorrelation based approach to estimate HR. ADA was performed on each signal independently. An iterative approach was then used to select the best heartrate of the three estimates. The technique is based on that of [11] where the HR estimate with the smallest difference from the HR estimate at the previous measurement instance was selected as the preferred output. This was enabled by the relative quasiperiodic nature of the heart such that the timing of each heartbeat is generally similar to that of the last, plus some small variability. The iteration was initialized for each file by using the average heart rate across all estimations for that file. This process enabled the algorithm to be less sensitive to outliers in each individual method.

E. EVALUATION

The performance of each algorithm depended on the severity of the motion artifacts. Therefore, to provide a robust view of the performance and its limitations, the algorithms were evaluated on a range of varying difficulties by adjusting the strength of the noise. This process was uniquely enabled by our artificially corrupted dataset as the noise could be manipulated with a strength coefficient when mixed with the clean data. Using this platform, the algorithm was then evaluated in three stages.

First, we evaluated how well the signal is reconstructed after decomposition. Since the decomposition stage can be the most computationally expensive and consequently the most significant step, it was important to evaluate the structural similarity. For this approach, we compared the reconstructed signal to the clean SCG waveform. Pearson's squared correlation coefficient (r^2) was used as a validation metric to measure the structural similarity across each test file.

Next, the decomposition methods were evaluated when assisted with ECG. Algorithms assisted by concurrent ECG can improve the noise tolerance by exploiting the more motion-tolerant electrical connections to produce clean waveforms. Most current motion artifact methods pair SCG with ECG to improve performance [27], [30], [31]. They commonly utilize ensemble averaging to mitigate the stochastic nature of motion artifacts. When paired with a decomposition technique, they can produce highly effective results. In this work, we compared each decomposition method when used in an ensemble average to evaluate to using the same structural similarity metrics. Cardiac heartbeats were segmented based on ECG-R peak, then collected into an ensemble and an average heartbeat was produced. A varying number of heartbeats in ECG-derived ensemble averages evaluated the impact of ensemble averaging as larger ensemble sizes should minimize non-periodic components. These ensembles were compared with the same ensemble average of the raw clean waveform.

The latter stages can be more destructive to the overall structure of the signal; however, they are used with the assumption that they suppress the motion artifact more than destroying the SCG. Therefore, at this stage, comparing structural similarity was not a valid approach as the structure would be significantly changed. Instead, we used HR estimation as both a verification tool, and a practical application. HR was estimated using the ADA algorithm and compared to the reference ECG-derived HR using Pearson's squared correlation coefficient. HR estimations were evaluated after each individual stage of the algorithm and were executed across a varying range of motion artifact strength.

III. RESULTS

A. DECOMPOSITION

The decomposition methods were evaluated on the artificially corrupted dataset for their ability to reconstruct the SCG waveform. Fig. 6 shows the average r^2 for each method across a varying signal to noise ratio (SNR) by manipulating the motion artifact strength. The full-strength SNR observed was −27 dB. SNR was calculated using the reference SCG and the mixed corrupted data for each permutation. All methods were negatively impacted by increasing noise amplitude. The correlation coefficient from the signal after just the band pass filter is shown as a reference. Understandably, as the simplest approach, this had the lowest performing reconstruction with the lowest r^2 except in the case of very low motion artifact noise. This is a consequence of features of the cardiac waveform being lost in the lower frequency bands during decomposition. This loss could potentially be mitigated by adaptively including more modes in the reconstruction to increase the reliability at lower noise levels. For consistency, all the signals were reconstructed using a constant number of modes, as described in Section II-C. However, for lower noise levels, established SCG processing techniques are typically sufficient, and thus they are not the primary emphasis of this work.

The best performing methods were CEEMDAN and MODWT as they had the highest r^2 for signal reconstruction. MODWT performed slightly better than CEEMDAN, particularly as it had a higher correlation at stronger noise levels. In this range, we can see that MODWT and CEEMDAN outperformed EMD and EEMD, which have been previously used for motion artifact removal in SCG [30], [31].

In addition to outperforming the EMD-based methods on an accuracy level, MODWT was much faster than the ensemble-based approaches, with a computation time approximately 128 times faster than CEEMDAN and 463 times faster than EEMD. The computation times for processing one minute of data and their corresponding

IEEE Journal of Translational Engineering in Health and Medicine

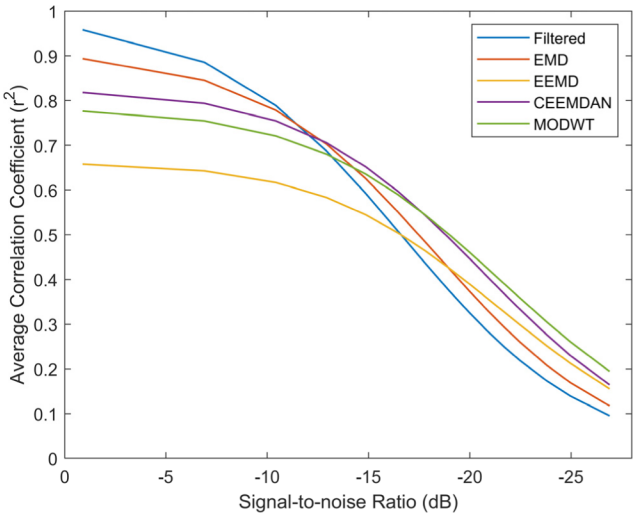

FIGURE 6. Quality of reconstruction showing the average correlation coefficient (r^2) for baseline filtering (blue), EMD (red), EEMD (yellow), CEEMDAN (purple), and MODWT (green).

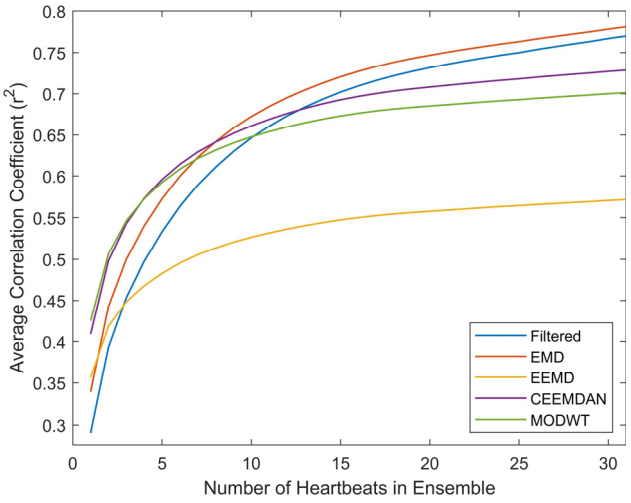

FIGURE 7. Average correlation coefficient for each ensemble average over an increasing number of heartbeats used in each ensemble. Shown for the reconstruction methods using filtering (blue), EMD (red), EEMD (yellow), CEEMDAN (purple), and MODWT (green).

correlations are shown in Table 1 at a SNR of –20.9 dB. The choice of this SNR ensured an adequate level of noise for evaluation under challenging circumstances, while still allowing each method to yield discernible results. The computation times of the ensemble-based methods could be improved by using fewer realizations; however, this would likely cause a reduction in the accuracy of the methods.

TABLE 1. Computational timing.

Method	Signal Correlation (r^2)	Computation Time
MODWT	0.4242	0.1047 s
CEEMDAN	0.4057	13.372 s
EEMD	0.3571	48.512 s
EMD	0.3307	0.0160 s
Filtering	0.2843	0.0029 s

B. ECG-ASSISTED RECONSTRUCTION

ECG, as a more motion-tolerant signal, was used to assist the decomposition methods in reconstruction of the SCG signal. The reconstruction was calculated at a SNR of –20.9 dB. Fig. 7 shows the results for each of the decomposition and baseline filtering approaches, when compared to the same ensemble.

The results show that regardless of the method used, the reconstruction correlation increased when the number heartbeats in the ensemble increased. This can be attributed to the motion artifacts being non-periodic with respect to the quasi-periodicity of the cardiac signal. This showed that ensemble averaging can be used as a tool to minimize motion artifacts, even without decomposition.

Additionally, it showed that when the ensemble size was large, most of the decomposition methods did not offer any improvement than bandpass filtering. The results were similar to the scenario in Fig. 6 when there was very low motion artifact noise, and the decomposition stage also provided no benefit over filtering. This is a consequence of cardiac features being lost in the lower bands of the decomposition. These features are preserved in the bandpass filtering and the ensemble approach reduced the motion artifacts.

C. HEART RATE ESTIMATION

A common application for SCG is HR monitoring, with a major advantage being its use in wearable scenarios. Therefore, HR estimation was used as both a verification tool, and a demonstration of practical utility. Fig. 8 shows the HR estimation performance from each stage of the proposed motion artifact reduction algorithm, on increasing noise levels. Unlike Fig. 6, this figure does not compare the methods in isolation, but shows how their use in each stage of the algorithm results in enhanced HR detection. Although any decomposition method could be used in the algorithm, MODWT was chosen as the desired technique due to the high reconstruction accuracy and low computational timing as demonstrated in section III-A. As seen when compared to the bandpass filtering reference, all stages significantly improved the HR detection accuracy. At low noise levels, all stages had a similar performance, whereas at higher noise levels, calculation after the TF masking stage improved the results from the previous MODWT stage. Interestingly, incorporating the NMF stage did not show significant overall improvement from the TF masking stage. This was likely a result of the method solving some motion artifact issues while creating new ones where it over attenuated the cardiac signal. However, what it did provide was an HR estimation where the failure points were often at different times from the MODWT or TF masking stage failure points. This allowed the selection algorithm to adaptively decide which of the three HR results it should output as a result. The selection stage resulted in

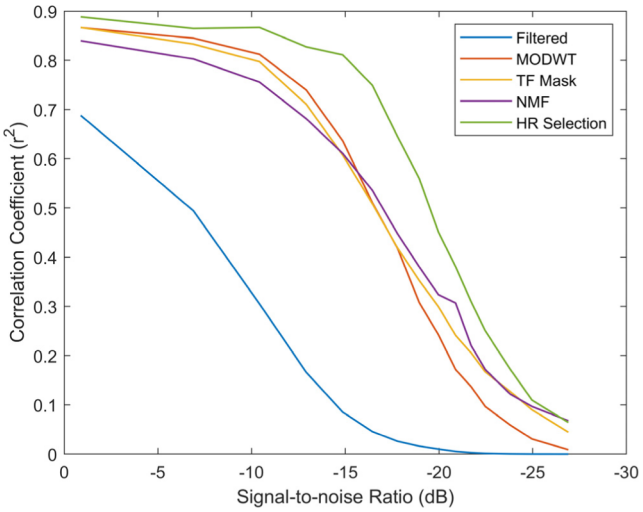

FIGURE 8. Heart rate estimation results showing the correlation coefficient (r^2) when compared against concurrent ECG-derived heart rate after baseline filtering (blue), and after each stage of the algorithm: after the MODWT stage (red), MODWT then CWT masking (yellow), MODWT then CWT masking then NMF (purple), and the iterative selection stage (green).

the highest r^2 across all SNR levels. However, at very high noise levels, even the selection algorithm did not improve the results enough for HR estimation as artifacts dominated the signal at all points and caused consistent large failures in all phases of the algorithm.

IV. DISCUSSION

The results of the study indicate that all the chosen decomposition methods improved the signal quality. Notably, the MODWT emerged as the most effective technique among the employed methods. While the combination of masking and NMF only minorly enhanced signal quality on their own when compared to MODWT, their joint utilization resulted in improved HR detection accuracy. For example, if we set a mean-absolute-error (MAE) tolerance of 5 bpm, the tolerance of the algorithm increases from −6.5 dB SNR from baseline filtering to −19 dB SNR after the algorithm.

When examining the performance at −15 dB, we observed a noteworthy improvement in HR r^2, elevating it from less than 0.1 to above 0.8. However, when evaluated at the original, full-strength of the back sensor at −27 dB, the method only marginally increased the r^2 from 0 to about 0.1. This highlights the success of the algorithm at lower noise levels, while showing challenges persist in some real-world scenarios. An innovative approach was adopted by leveraging an artificially corrupted dataset that represented real signals as it was generated using two real sources. This dataset offered a more manageable platform for analysis when compared to full-strength recordings, and enabled significant progress in a domain that was previously perceived as unattainable. It is crucial to note that, in the experiment, we intentionally subjected subjects to continuous walking, which represents a high-motion artifact scenario. In real-world applications, the average individual is fairly sedentary [48], engaging in a variety of lighter activities, such as sleeping, sitting, or light movements, and this sedentary behavior is even higher in hospitalized patients [49]. Therefore, this work enables SCG monitoring throughout most of the day for clinical and daily life applications.

A similar study measured a SNR of around −5 dB to −15 dB from subway vibrations [31]. Another study demonstrated an algorithm with a tolerance of 40 mill-g standard deviation of motion artifacts [25]. In our study, we observed an equivalent standard deviation value at −21 dB SNR. A third study reported mean squared energy of 0.02, 0.009, and 0.016 while walking on a treadmill at 1.3 m/s, a user-set pace, and a brisk pace, respectively [30]. Our study observed an equivalent energy at −23 dB, −20 dB, and −22 dB. Therefore, the full-strength of our recordings were consistently much stronger than other works. In the −15 dB to −20 dB range observed in these other studies, our algorithm is particularly well-suited for addressing motion artifacts in real-world scenarios, thereby reinforcing its practical applicability in everyday monitoring situations, and enabling its clinical use. Additionally, all three studies utilized ECG to reduce motion artifact, whereas our study is a standalone SCG-only approach. The nature of the walking surface and the impact exerted during locomotion can be identified as potential factors affecting signal quality. This study was conducted with subjects walking barefoot on a firm flooring, whereas factors such as shoes [50] or utilization of treadmills [51] can provide some shock-absorbing properties that dampen vibrations and could explain why this study had worse SNR than comparable studies.

We observed in Fig. 6 that simple filtering had the highest r^2 for very low motion artifact noise. Counterintuitively, it had a worse performance for HR than MODWT as seen in Fig. 8. As outlined in Section III-A, the diminished reconstruction performance in cases of low motion artifact noise can be attributed to the loss of features from the SCG waveform in the lower-frequency bands during decomposition. However, while this process removes some of the SCG signal, it also effectively eliminates more of the disruptive motion artifacts within this frequency range. We can conclude that 1) the lower frequency information may not be of crucial importance for HR estimation, and 2) the loss of this information is counterbalanced by the enhanced suppression of motion artifacts, ultimately resulting in a more dependable HR estimation.

Another important observation was that when the HR algorithm failed, it would deviate significantly from the actual HR. Incorporating outlier methods could potentially improve these results, however this was deemed outside the scope of this work as it would not create a fair comparison between the previously published HR algorithm. Additionally, the HR selection should be further verified in cases of arrhythmias where this approach could smooth variability and mask such pathologies.

Similarly, as the HR estimates were often either reasonably close or significantly off, it could be feasible to

intermittently monitor HR instead of continuous monitoring. In this approach, motion artifacts could be detected, and a signal quality index could selectively record HR during periods of high confidence where motion artifacts are more easily reduced.

Another method to improve noise tolerance would be to record ECG concurrently. ECG was shown to improve the reconstruction quality by incorporating ensemble averaging. The increase in r^2 directly correlated with the number of heartbeats used. However, using a larger number of heartbeats limits the beat-to-beat monitoring, while potentially smooths features which could be of importance to specific applications [30]. Additionally, HR monitoring is not possible with this technique but if ECG is being used, it could provide the HR information instead of SCG. The downside of this approach is the increased hardware complexity and more points of contact on the body. ECG-assisted SCG algorithms provide useful applications towards cardiac time interval detection such as the pre-ejection period or left-ventricular ejection time [29], [30], [31] where the number of heartbeats can be finetuned to the specific needs of the application. In such contexts, the concurrent use of SCG and ECG remains a valuable approach for a more comprehensive assessment of cardiac performance.

V. CONCLUSION

This study investigated EMD, EEMD, CEEMDAN and MODWT to mitigate motion artifacts in SCG signals. Of these, MODWT yielded the highest quality signals and faster decomposition. Additionally, a combined approach involving MODWT, TF masking, and NMF showed significant enhancements for HR estimation. Although the approach outperforms current state of the art, at high noise levels, this combined approach was still insufficient for implementation in a practical device. Therefore, to enable SCG recordings at higher noise levels, the adoption of an intermittent monitoring scheme, or motion-tolerant ECG should be incorporated. By addressing the challenges posed by motion artifacts, we effectively increase the versatility of SCG monitoring. Our results allow SCG measurements to be more accurate under motion artifacts, which therefore improve the reliability of insights into cardiovascular dynamics. This promotes the applicability of SCG to ambulatory scenarios, including clinical settings both in the hospital, and remote monitoring, thereby facilitating improved diagnosis of conditions like arrhythmias, ischemia, and heart failure. Moreover, this advancement enables the development of robust wearable devices that can be seamlessly integrated into daily life, allowing continuous monitoring and timely detection of cardiac abnormalities.

REFERENCES

[1] T. Vos et al., "Global burden of 369 diseases and injuries in 204 countries and territories, 1990–2019: A systematic analysis for the global burden of disease study 2019," *The Lancet*, vol. 396, no. 10258, pp. 1204–1222, 2020.

[2] M. D. Rienzo, G. Grassi, A. Pedotti, and G. Mancia, "Continuous vs intermittent blood pressure measurements in estimating 24-hour average blood pressure," *Hypertension*, vol. 5, no. 2, pp. 264–269, Mar. 1983.

[3] A. Y. A. Amer et al., "Vital signs prediction and early warning score calculation based on continuous monitoring of hospitalised patients using wearable technology," *Sensors*, vol. 20, no. 22, p. 6593, Nov. 2020.

[4] F. Lamonaca, G. Polimeni, K. Barbé, and D. Grimaldi, "Health parameters monitoring by smartphone for quality of life improvement," *Measurement*, vol. 73, pp. 82–94, Sep. 2015.

[5] D. Duncker et al., "Smart wearables for cardiac monitoring—Real-world use beyond atrial fibrillation," *Sensors*, vol. 21, no. 7, p. 2539, Apr. 2021.

[6] J. Dunn, R. Runge, and M. Snyder, "Wearables and the medical revolution," *Personalized Med.*, vol. 15, no. 5, pp. 429–448, Sep. 2018, doi: 10.2217/pme-2018-0044.

[7] I. C. Jeong, D. Bychkov, and P. C. Searson, "Wearable devices for precision medicine and health state monitoring," *IEEE Trans. Biomed. Eng.*, vol. 66, no. 5, pp. 1242–1258, May 2019.

[8] J. M. Zanetti and K. Tavakolian, "Seismocardiography: Past, present and future," in *Proc. 35th Annu. Int. Conf. IEEE Eng. Med. Biol. Soc. (EMBC)*, Jul. 2013, pp. 7004–7007.

[9] A. Taebi, B. Solar, A. Bomar, R. Sandler, and H. Mansy, "Recent advances in seismocardiography," *Vibration*, vol. 2, no. 1, pp. 64–86, Jan. 2019, doi: 10.3390/vibration2010005.

[10] Y. D'Mello et al., "Autocorrelated differential algorithm for real-time seismocardiography analysis," *IEEE Sensors J.*, vol. 19, no. 13, pp. 5127–5140, Jul. 2019.

[11] D'Mello et al., "Real-time cardiac beat detection and heart rate monitoring from combined seismocardiography and gyrocardiography," *Sensors*, vol. 19, no. 16, p. 3472, Aug. 2019.

[12] E. M. I. Johnson et al., "Detecting aortic valve-induced abnormal flow with seismocardiography and cardiac MRI," *Ann. Biomed. Eng.*, vol. 48, no. 6, pp. 1779–1792, Jun. 2020.

[13] S. Mehrang et al., "End-to-end sensor fusion and classification of atrial fibrillation using deep neural networks and smartphone mechanocardiography," *Physiol. Meas.*, vol. 43, no. 5, May 2022, Art. no. 055004.

[14] M. M. H. Shandhi, J. Fan, J. A. Heller, M. Etemadi, L. Klein, and O. T. Inan, "Estimation of changes in intracardiac hemodynamics using wearable seismocardiography and machine learning in patients with heart failure: A feasibility study," *IEEE Trans. Biomed. Eng.*, vol. 69, no. 8, pp. 2443–2455, Aug. 2022, doi: 10.1109/TBME.2022.3147066.

[15] R. S. Crow, P. Hannan, D. Jacobs, L. Hedquist, and D. M. Salerno, "Relationship between seismocardiogram and echocardiogram for events in the cardiac cycle," *Amer. J. Noninvasive Cardiol.*, vol. 8, no. 1, pp. 39–46, 1994.

[16] K. Sørensen, S. E. Schmidt, A. S. Jensen, P. Søgaard, and J. J. Struijk, "Definition of fiducial points in the normal seismocardiogram," *Sci. Rep.*, vol. 8, no. 1, p. 15455, Oct. 2018, doi: 10.1038/s41598-018-33675-6.

[17] M. Di Rienzo, E. Vaini, P. Castiglioni, P. Meriggi, and F. Rizzo, "Beat-to-beat estimation of LVET and QS2 indices of cardiac mechanics from wearable seismocardiography in ambulant subjects," in *Proc. 35th Annu. Int. Conf. IEEE Eng. Med. Biol. Soc. (EMBC)*, Jul. 2013, pp. 7017–7020.

[18] Y. D'Mello et al., "Identification of the vibrations corresponding with heart sounds using vibrational cardiography," in *Proc. 42nd Annu. Int. Conf. IEEE Eng. Med. Biol. Soc. (EMBC)*, Jul. 2020, pp. 17–20.

[19] H. Ashouri, S. Hersek, and O. T. Inan, "Universal pre-ejection period estimation using seismocardiography: Quantifying the effects of sensor placement and regression algorithms," *IEEE Sensors J.*, vol. 18, no. 4, pp. 1665–1674, Feb. 2018.

[20] M. M. H. Shandhi, B. Semiz, S. Hersek, N. Goller, F. Ayazi, and O. T. Inan, "Performance analysis of gyroscope and accelerometer sensors for seismocardiography-based wearable pre-ejection period estimation," *IEEE J. Biomed. Health Informat.*, vol. 23, no. 6, pp. 2365–2374, Nov. 2019.

[21] V. G. Ganti et al., "Wearable seismocardiography-based assessment of stroke volume in congenital heart disease," *J. Amer. Heart Assoc.*, vol. 11, no. 18, Sep. 2022, Art. no. e026067.

[22] J. Skoric et al., "Respiratory modulation of sternal motion in the context of seismocardiography," *IEEE Sensors J.*, vol. 22, no. 13, pp. 13055–13066, Jul. 2022.

[23] V. G. Motti and K. Caine, "Human factors considerations in the design of wearable devices," in *Proc. Hum. Factors Ergonom. Soc. Annu. Meeting*, 2014, vol. 58, no. 1, pp. 1820–1824.

[24] C. Ferguson, L. D. Hickman, S. Turkmani, P. Breen, G. Gargiulo, and S. C. Inglis, "'Wearables only work on patients that wear them': Barriers and facilitators to the adoption of wearable cardiac monitoring technologies," *Cardiovascular Digit. Health J.*, vol. 2, no. 2, pp. 137–147, 2021.

[25] C. Yang and N. Tavassolian, "Motion artifact cancellation of seismocardiographic recording from moving subjects," *IEEE Sensors J.*, vol. 16, no. 14, pp. 5702–5708, Jul. 2016.

[26] A. Taebi, "Noise cancellation from vibrocardiographic signals based on the ensemble empirical mode decomposition," *J. Appl. Biotechnol. Bioeng.*, vol. 2, no. 2, p. 24, Feb. 2017.

[27] C. Yang and N. Tavassolian, "An independent component analysis approach to motion noise cancelation of cardio-mechanical signals," *IEEE Trans. Biomed. Eng.*, vol. 66, no. 3, pp. 784–793, Mar. 2019.

[28] D. Berwal, C. Vandana, S. Dewan, C. Jiji, and M. S. Baghini, "Motion artifact removal ambulatory ECG signal heart rate variability analysis," *IEEE Sensors J.*, vol. 19, no. 24, pp. 12432–12442, Sep. 2019.

[29] M. Di Rienzo et al., "Wearable seismocardiography: Towards a beat-by-beat assessment of cardiac mechanics in ambulant subjects," *Autonomic Neurosci.*, vol. 178, nos. 1–2, pp. 50–59, Nov. 2013.

[30] A. Q. Javaid et al., "Quantifying and reducing motion artifacts in wearable seismocardiogram measurements during walking to assess left ventricular health," *IEEE Trans. Biomed. Eng.*, vol. 64, no. 6, pp. 1277–1286, Jun. 2017.

[31] D. J. Lin, J. P. Kimball, J. Zia, V. G. Ganti, and O. T. Inan, "Reducing the impact of external vibrations on fiducial point detection in seismocardiogram signals," *IEEE Trans. Biomed. Eng.*, vol. 69, no. 1, pp. 176–185, Jan. 2022.

[32] K. Pandia, S. Ravindran, R. Cole, G. Kovacs, and L. Giovangrandi, "Motion artifact cancellation to obtain heart sounds from a single chest-worn accelerometer," in *Proc. IEEE Int. Conf. Acoust., Speech Signal Process.*, Mar. 2010, pp. 590–593.

[33] S. Yu and S. Liu, "A novel adaptive recursive least squares filter to remove the motion artifact in seismocardiography," *Sensors*, vol. 20, no. 6, p. 1596, Mar. 2020.

[34] T. Choudhary, L. N. Sharma, and M. K. Bhuyan, "Automatic detection of aortic valve opening using seismocardiography in healthy individuals," *IEEE J. Biomed. Health Informat.*, vol. 23, no. 3, pp. 1032–1040, May 2019.

[35] P. K. Jain and A. K. Tiwari, "A novel method for suppression of motion artifacts from the seismocardiogram signal," in *Proc. IEEE Int. Conf. Digit. Signal Process. (DSP)*, Oct. 2016, pp. 6–10.

[36] E. Aboulezz et al., "Analyzing heart rate estimation from vibrational cardiography with different orientations," in *Proc. 42nd Annu. Int. Conf. IEEE Eng. Med. Biol. Soc. (EMBC)*, Jul. 2020, pp. 2638–2641.

[37] C. Yang and N. Tavassolian, "Motion noise cancellation in seismocardiogram of ambulant subjects with dual sensors," in *Proc. 38th Annu. Int. Conf. IEEE Eng. Med. Biol. Soc. (EMBC)*, Aug. 2016, pp. 5881–5884.

[38] N. E. Huang et al., "The empirical mode decomposition and the Hilbert spectrum for nonlinear and non-stationary time series analysis," *Proc. Roy. Soc. Lond. Ser. Math. Phys. Eng. Sci.*, vol. 454, no. 1971, pp. 903–995, Mar. 1998, doi: 10.1098/rspa.1998.0193.

[39] Z. Wu and N. E. Huang, "Ensemble empirical mode decomposition: A noise-assisted data analysis method," *Adv. Adapt. Data Anal.*, vol. 1, pp. 1–41, Jan. 2009.

[40] M. E. Torres, M. A. Colominas, G. Schlotthauer, and P. Flandrin, "A complete ensemble empirical mode decomposition with adaptive noise," in *Proc. IEEE Int. Conf. Acoust., Speech Signal Process. (ICASSP)*, May 2011, pp. 4144–4147.

[41] D. B. Percival and A. T. Walden, *Wavelet Methods for Time Series Analysis*. Cambridge, U.K.: Cambridge Univ. Press, 2000.

[42] O. Yilmaz and S. Rickard, "Blind separation of speech mixtures via time-frequency masking," *IEEE Trans. Signal Process.*, vol. 52, no. 7, pp. 1830–1847, Jul. 2004.

[43] T. Virtanen, "Monaural sound source separation by nonnegative matrix factorization with temporal continuity and sparseness criteria," *IEEE Trans. Audio, Speech Lang., Process.*, vol. 15, no. 3, pp. 1066–1074, Mar. 2007.

[44] Y.-X. Wang and Y.-J. Zhang, "Nonnegative matrix factorization: A comprehensive review," *IEEE Trans. Knowl. Data Eng.*, vol. 25, no. 6, pp. 1336–1353, Jun. 2013.

[45] D. Lee and H. S. Seung, "Algorithms for non-negative matrix factorization," in *Proc. Adv. Neural Inf. Process. Syst.*, vol. 13, 2000, pp. 1–7.

[46] M. W. Berry, M. Browne, A. N. Langville, V. P. Pauca, and R. J. Plemmons, "Algorithms and applications for approximate nonnegative matrix factorization," *Comput. Statist. Data Anal.*, vol. 52, no. 1, pp. 155–173, Sep. 2007.

[47] A. Taebi and H. Mansy, "Time-frequency distribution of seismocardiographic signals: A comparative study," *Bioengineering*, vol. 4, no. 4, p. 32, Apr. 2017.

[48] C. E. Matthews et al., "Sedentary behavior in United States adults: Fall 2019," *Med. Sci. Sports Exercise*, vol. 53, no. 12, p. 2512, 2021.

[49] U. Jasper, L. Yadav, J. Dollard, A. D. Jadczak, S. Yu, and R. Visvanathan, "Sedentary behaviour in hospitalised older people: A scoping review," *Int. J. Environ. Res. Public Health*, vol. 17, no. 24, p. 9359, Dec. 2020, doi: 10.3390/ijerph17249359.

[50] M. A. Lafortune and E. M. Hennig, "Cushioning properties of footwear during walking: Accelerometer and force platform measurements," *Clin. Biomech.*, vol. 7, no. 3, pp. 181–184, Aug. 1992.

[51] C. Milgrom, "Are overground or treadmill runners more likely to sustain tibial stress fracture?" *Brit. J. Sports Med.*, vol. 37, no. 2, pp. 160–163, Apr. 2003.